Journal of Ceramic Processing Research. Vol. 17, No. 3, pp. 191~196 (2016)

J O U R N A L O F
Ceramic Processing Research

One step synthesis and densification of Titanium-silicon compounds by a spark plasma sintering method and their mechanical properties

Hyun-Kuk Park[a,b], Ik-Hyun Oh[a], Jun-Ho Jang[a], Hyun-Taek Shon[a], Ho-Sung Kim[a] and In-Jin Shon[b,*]

[a]*Korea Institute of Industrial Technology (KITECH), Automotive Components Group, Gwang-Ju, 500-480 Korea*

[b]*Division of Advanced Materials Engineering and Research Center of Advanced Materials Development, Chonbuk National University, 664-14 Deokjin-dong 1-ga, Deokjin-gu, Jeonju, Jeonbuk 561-756, Korea*

Spark plasma sintering (SPS method) method was used to densify Ti-x wt.% Si compounds materials from Ti and Si powders. Sintered Ti and Ti-x wt.%) Si materials were almost entirely dense with a relative density of up to 100% after applying an electric current for 11 min under 60 MPa of pressure at 1000 ºC. The average grain size of Ti_5Si_3 compound obtained from Ti-10 wt.% Si powder was of about 35 nm with a hardness of ~ 640 kg/mm^2.

Key words: Spark plasma sintering, Ti-Si compounds, Mechanical property, Rapid sintering.

Introduction

Over the past 20 years, intermetallic compounds have gained an increasing amount of attention for potential use in the aerospace industry due to their high melting point, low density, high strength, and excellent resistance to oxidation [1-5]. Ti_5Si_3 is one of such intermetallic compounds, and it is considered to be promising for use in high-temperature structural applications. This compound has a high melting temperature (2403 K), low density (4.23 g/cm^3), high hardness (11.3 GPa), good strength at elevated temperatures, excellent creep resistance, and high oxidation resistance [6-8]. However, its complex hexagonal structure results in very low fracture toughness at room temperature due to low symmetry and highly covalent bonding that increase the Peierls stress [9].

A number of similar high-temperature, dense composites have been prepared by using a multistep processes [10, 11], and Ti_5Si_3 has generally been processed by using a variety of methods, including arc melting of the Ti and Si pieces, hot isostatic pressing for Ti_5Si_3 powders obtained by crushing the reaction sintered product, mechanical alloying of Ti and Si powders, and element powder metallurgy. When conventional sintering processes are used to sinter nano-sized powders, the concomitant grain growth leads to the destruction of the nanostructure.

Therefore, attention has been focused on consolidation methods where grain growth can be eliminated or significantly reduced. To this end, rapid sintering methods have been extensively used to sinter nano-sized powders. The most obvious advantage of rapid sintering is that fast heating and cooling rates can be achieved, and the short dwell time leads to bypassing low-temperature, non-densifying mass transport (e.g., surface diffusion) [12, 13]. Therefore, the grain growth during sintering must be controlled in order to ensure the commercial success of nanostructured Ti-Si composites.

Spark plasma sintering has been successfully employed to synthesize and densify a variety of materials from their respective elements in one step and in a relatively short period of time. This method can be used to synthesize a variety of ceramics and composites, including $MoSi_2$-ZrO2, WSi_2 and its composites, and WC-Co hard materials [14-19]. These materials are generally characterized by a low

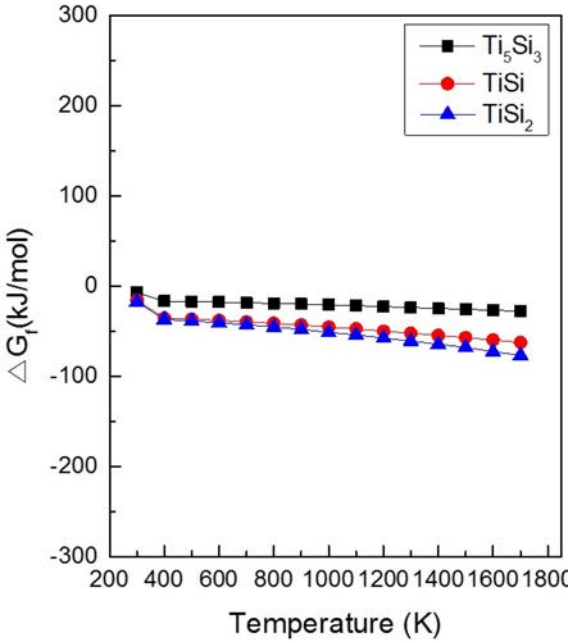

Fig. 1. Temperature dependence of the Gibbs free energy variation by interaction of the Ti phase with Si.

*Corresponding author:
Tel : +82-63-270-2381
Fax: +82-63-270-2389
E-mail: ijshon@chonbuk.ac.kr

adiabatic combustion temperature and cannot be synthesized directly by self-propagating high-temperature synthesis (SHS). Fig. 1 shows that when the Ti phase is in contact with Si, the formation of Ti_5Si_3, TiSi and $TiSi_2$ phases is thermodynamically possible through solid-state displacement according to the following equation:

$$5Ti + 3Si \rightarrow Ti_5Si_3$$
$$Ti + Si \rightarrow TiSi$$
$$Ti + 2Si \rightarrow TiSi_2$$

In this study, spark plasma sintering method was used to produce dense nano-crystalline Ti_5Si_3 composites from mixtures of mechanically activated Ti and Si powders through a one-step process within 11 minutes, and the mechanical properties of the resulting materials were investigated.

Experimental Procedure

In this study, 99.98% pure titanium (−800 mesh, Kojundo Chem. Products) and 99.5% pure silicon (−325 mesh, Alfa Products) powders were used as starting materials. The FE-SEM images and XRD patterns of the raw materials are shown in Fig. 2, and only Ti and Si peaks appear in the XRD patterns. Ti and Ti-1 ~ 10 wt.% Si powder mixtures were first milled at 250 RPM for 10 hrs with a high-energy planetary ball mill (Pulverisette-5). The mill contained tungsten carbide balls with diameters of 6 and 10 mm in a sealed cylindrical stainless steel vial with alcohol. The balls-to-powder weight ratio was 10 : 1, and that of the alcohol-to-powder was 2 : 1.

Fig. 3 shows the XRD patterns of the milled powders. The particle size and the internal strain of the ball-milled powders were calculated using Stokes and Wilson's formula [20]:

$$b = b_d + b_e = k\lambda /(d\cos\theta) + 4\varepsilon\tan\theta \quad (1)$$

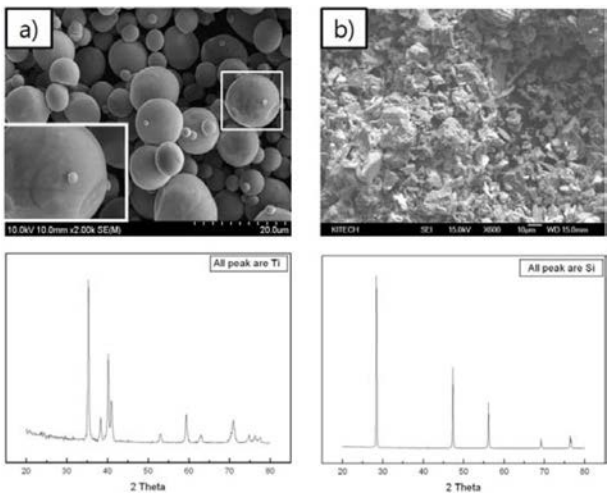

Fig. 2. FE-SEM images and XRD patterns of raw materials : a) Ti and b) Si.

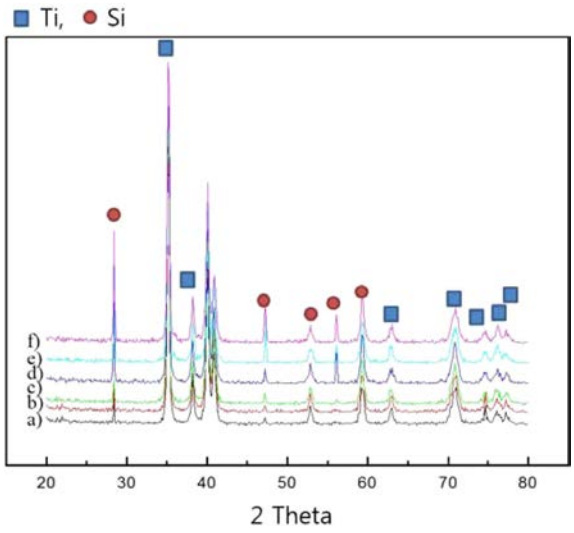

Fig. 3. XRD patterns of Ti-x wt.%Si powders milled using high-energy ball for various Si content : a) 0%Si, b) 1% Si, c) 2% Si, d) 3% Si, e) 5% Si and f) 10% Si.

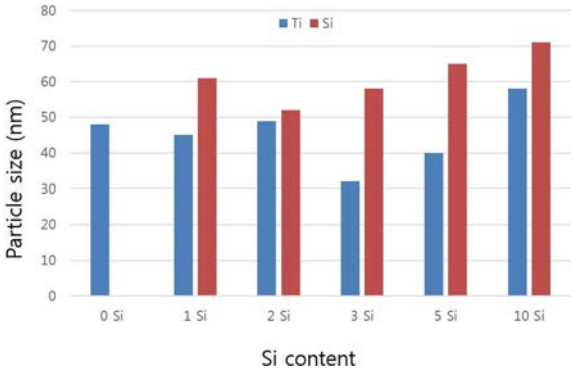

Fig. 4. Particle size of the Ti-Si powder high-energy ball milled for various Si content.

where b is the full width at half-maximum (FWHM) of the diffraction peak after instrumental correction; b_d and b_e are the FWHM for the small grain size and the internal strain, respectively; k is a constant with a value of 0.9; λ is X-ray radiation wavelength; d and ε are the grain size and the internal strain, respectively; and θ is the Bragg angle. b and bs follow Cauchy's form as $B_0 = b + b_s$, where B_0 and b_s are the FWHM of the broadened Bragg peaks and the Bragg peaks of the standard sample, respectively. Fig. 4 shows the average particle size of the Ti-x wt.% Si powders after milling, with that of Ti at about 48, 45, 49, 32, 40, 58 nm and that of Si at 0, 61, 52, 58, 65, 71 nm.

After milling, the mixed powders were placed in a graphite die (outside diameter, 30 mm; inside diameter, 10 mm; height, 40 mm) that was then placed into a spark plasma sintering system (Sumitomo Coal Mining, Japan). The SPS device was configured with a 25 V, 1000 A DC power supply and a 10 ton uniaxial press. A pulsed current ran through the sample and die for 12 ms with an off time of 2 ms.

Fig. 5 shows a schematic diagram for the SPS

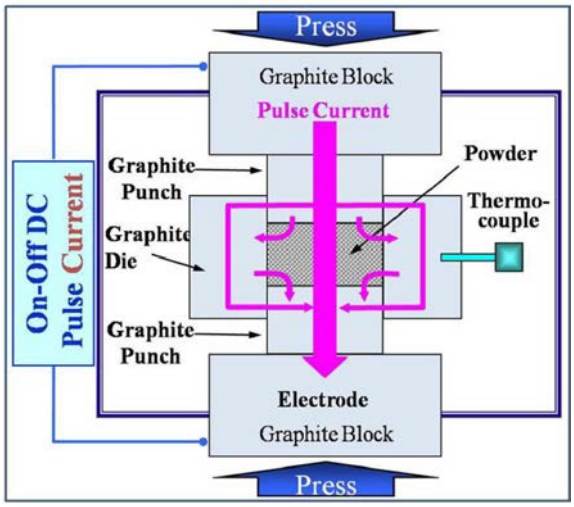

Fig. 5. Schematic diagram of apparatus for Spark Plasma Sintering.

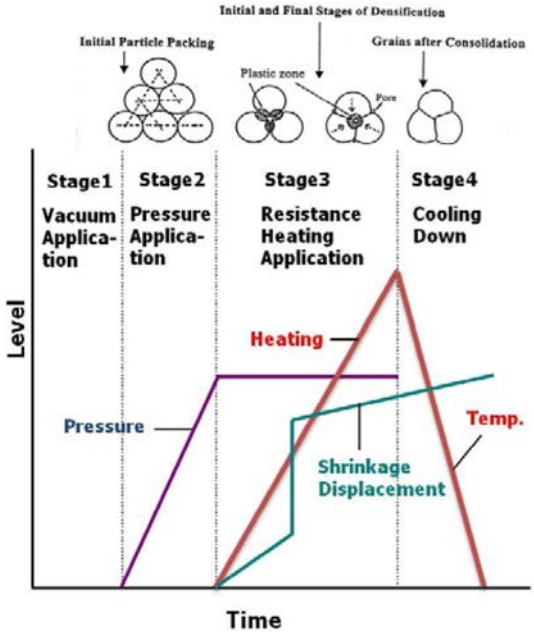

Fig. 6. Schematic representation of the temperature, Pressure and shrinkage displacement profile during SPS.

process. First, the system was evacuated to a 6 Pa vacuum, and uniaxial pressure was applied at 60 MPa. Then, a pulsed current was activated and maintained until the densification rate was negligible, as indicated by the observed shrinkage of the sample, which was monitored in real time with a linear gauge that assessed vertical displacement. The temperature was measured using a k-type thermo-couple since the electrical and thermal conductivities of the compact, its relative density, and the temperature on the surface and in the center of the sample could be different depending on the heating rate, which in this case was set to approximately 100 °C/min. When the process was complete, the current was turned off, and the sample was allowed to cool to room temperature. The entire SPS densification process consists of four major control stages: chamber evacuation, pressure application, power application, and cool down (Fig. 6).

The relative densities of the sintered samples were measured by using the Archimedes method. The product samples were polished and etched using HF (10 vol. %), HNO_3 (10 vol. %) and H_2O (80 vol. %) for 30 sec at room temperature, and X-ray diffraction (XRD) and field-emission scanning electron microscopy (FE-SEM) were carried out to analyze the compositional and microstructural properties of the products. The Vickers hardness for the synthesized samples was measured by performing indentation tests with a 10 kg load and a 15 sec dwell time.

Results and Discussion

Fig. 7 shows the variation in the shrinkage displacement and temperature with respect to sintering time for the Ti and Ti-x wt.%Si compounds sintered via SPS with 60 MPa of pressure. When an electric current is applied, the shrinkage displacement is nearly constant at up to 200 °C and then abruptly increases at above that temperature. When the temperature reaches about 1000 °C, the densification rate becomes nearly negligible, and the samples densify to the maximum theoretical density at about 650 sec, as will be further discussed below. The

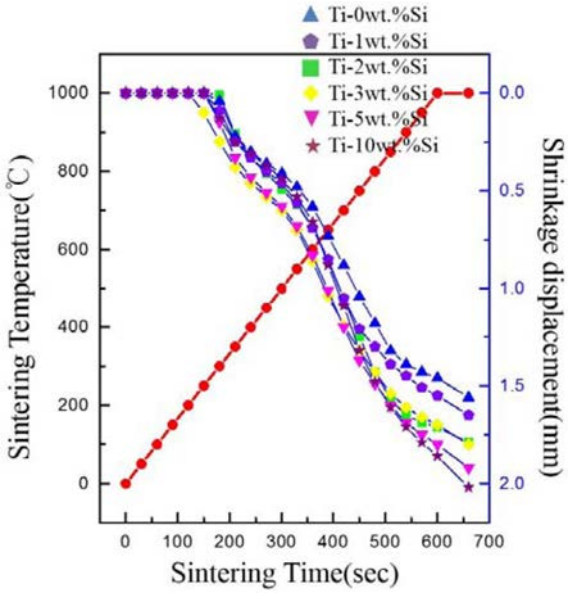

Fig. 7. Variation of temperature and shrinkage displacement with sintering time during SPS of Ti-x wt.%Si compounds.

sintered densities of the Ti and Ti-1, 2, 3, 5, 10 wt. %Si samples were 4.507, 4.465, 4.424, 4.384, 4.306 and 4.122 g/cm^3, respectively. The measurements for the shrinkage displacement and the initial height of the powder compact (Fig. 7) were used to measure the height variation of the powdered compact with relative precision as $\Delta L = L_r - L_0 < 0$, where L_T is the instantaneous height

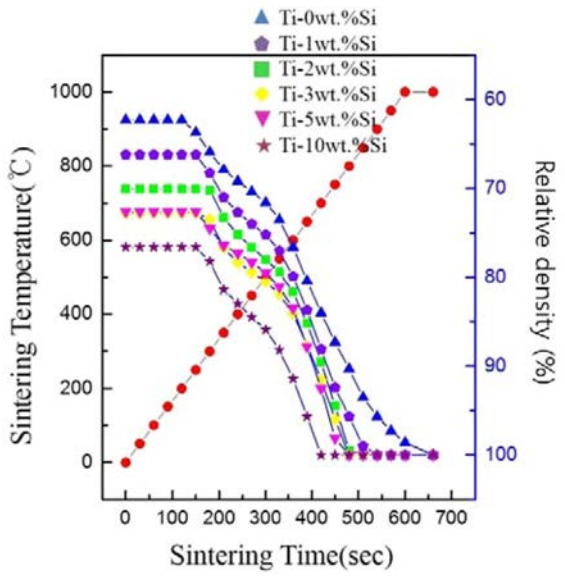

Fig. 8. Variation of temperature and relative density with sintering time during SPS of Ti-x wt.%Si compounds.

and L_0 is the initial height of the powder compact. Therefore, the instantaneous relative density D can be computed as [21]

$$D_T = (L_f / L_T)D_f \quad (2)$$

Where D_T is the instantaneous relative density, L_f is the final height, L_T is the instantaneous height, and D_f is the final relative density.

Fig. 8 shows the variations in the temperature and the relative density of the Ti and Ti-x wt.% Si compounds with respect to heating time during sintering via SPS at 60 MPa. The relative densities were dependent on the load added to the initial mold, but the relative density changed at about 300 ºC, and then abruptly increased as the temperature increased further. When the temperature reached about 600 ºC, the relative density was almost the maximum for the Ti-10 wt.% Si sample. However, the pure Ti sample did not achieve the maximum density at 680 ºC. As the Si contents increased, the sintering rate and the densification rate of the samples quickly increased, as shown Figs. 7 and 8. The abrupt increase in the shrinkage displacement at the ignition temperature is a result of the increase in the density due to the change in the molar volume associated with the formation of Ti_5Si_3 and the consolidation of the product.

The temperature is measured at the surface of the die, and it is therefore likely to be different from that in the middle of the sample. Thus, the onset of the reaction that formed the composite may occur at a higher temperature than at the observed value of 250 ºC. The XRD patterns for the series of binary Ti-x wt.% Si alloys are shown in Fig. 9. Pure Ti was comprised entirely of a hexagonal á phase, and the Ti-1 ~ 5 wt.%Si alloys contained a single α-Ti phase at room temperature with a minor phase (TiSi, $TiSi_2$ and Ti_5Si_3). The Ti-10 wt.%Si sample contained intermetallic Ti_5Si_3, and the XRD patterns indicated that as the Si content increased, the quantity of Ti_5Si_3 increased as well, with particularly high content for the Ti-10 wt. %Si sample. The presence of $TiSi_2$ and TiSi suggests that there is a deficiency of Ti.

The structural parameters, i.e., the average grain size of Ti_5Si_3 obtained from the Stokes and Wilson formula [20], are shown in Fig. 10. As the Si content increased, the grain size for the Ti and Ti-x wt.% Si samples decreased slightly. The mechanism through which a higher density and a finer structure can obtained in a short amount of time through the use of pulsed current heating with pressure is not well understood. However,

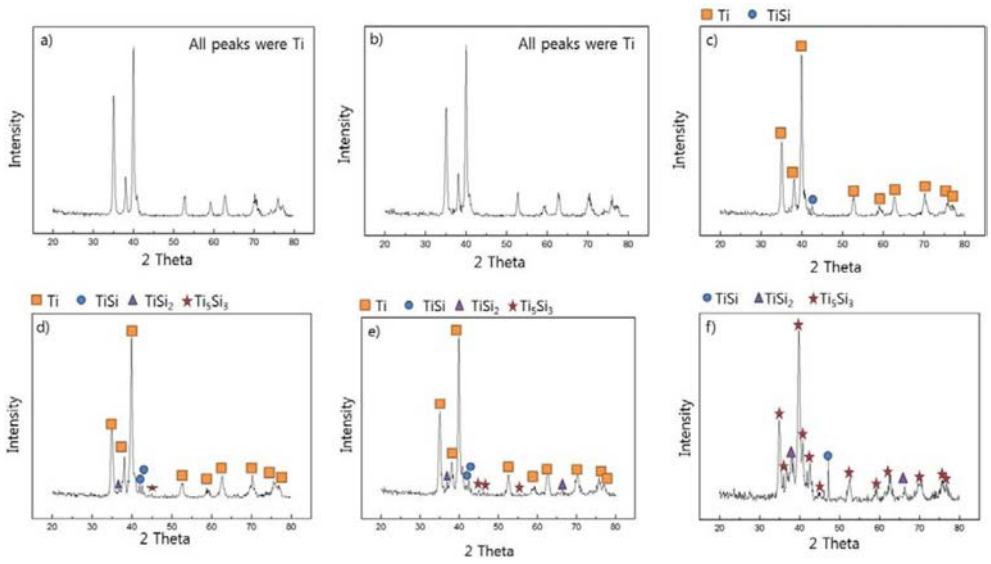

Fig. 9. XRD patterns of Ti-Si compounds sintered by SPS : a) Pure Ti, b) Ti-1wt.%Si, c) Ti-2wt.%Si, d) Ti-3wt.%Si, e) Ti-5wt.%Si and f) Ti-10wt.%Si.

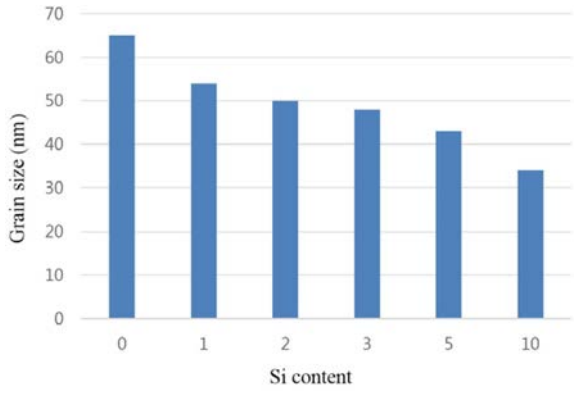

Fig. 10. Grain size of the Ti-x wt.%Si compounds from high-energy ball milled powder for various Si content.

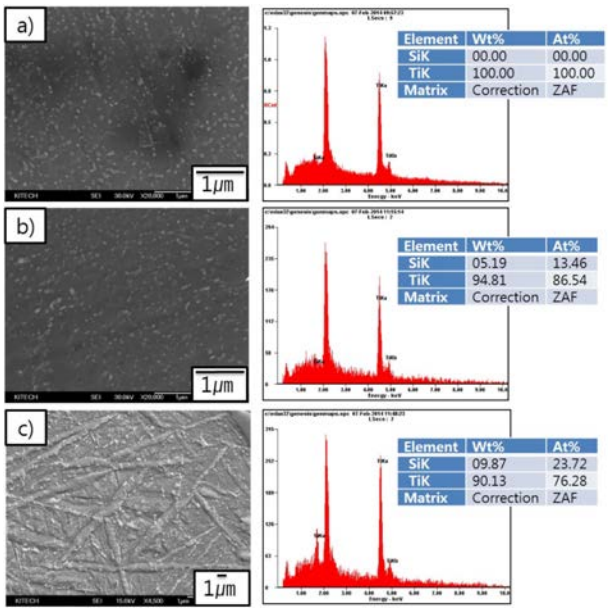

Fig. 11. FE-SEM images of etched surface of Ti-x wt.%Si compounds for various Si content : a) 0% Si, b) 5% Si and c) 10% Si.

it appears that the densification via SPS may be attributed to a combination of the electrical discharge and the pressure that is applied.

Fig. 11 shows FE-SEM images of the etched surface as well as an EDX analysis of the Ti and Ti-Si samples with various Si contents at 0 wt. % Si, 5 wt.% Si and 10 wt.% Si. The Ti-Si phase diagram indicates a eutectic composition at approximately 8 wt.%. In this study, the Ti-0 ~ 5 wt.%Si alloys correspond to hypoeutectic compositions with a hexagonal α phase while the Ti-10 wt.%Si alloy was within the hypereutectic composition range and exhibited the corresponding microstructural features including massive pro-eutectic Ti_5Si_3 phase domains and typical α-Ti + Ti_5Si_3 lath structures.

The Vickers hardness measurements were taken on polished sections of the Ti-Si samples by using a 10 kgf load with a dwell time of 15 sec. Fig. 12 shows the Vickers hardness of the Ti-Si samples with respect to Si content. As the Si content increased, the Vickers

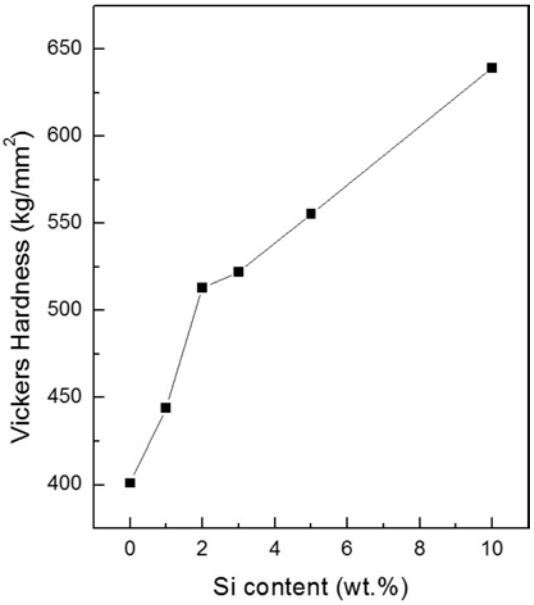

Fig. 12. Vickers hardness of Ti-x wt%Si compounds for Si content.

hardness of the Ti-x wt.%Si samples increased, likely as a result of the increase in TiSi, $TiSi_2$ and Ti_5Si_3 phases due to the increase in Si.

Summary

The Ti-x wt.%Si materials were rapidly consolidated using via SPS method with high-energy ball milled powders (Ti + Si). After milling, the Ti-10 wt.%Si powder exhibited a grain size of about 60 nm. An almost fully dense Ti-10wt.%Si sample was obtained within 11 min. The densification temperature of Ti was remarkably reduced by adding Si, and the relative densities of the composites were of about 100% at an applied pressure of 60 MPa at 1000 ºC. The grain size of Ti_5Si_3 was of about 35 nm, and the nano-structures did not exhibit grain growth during sintering via SPS. The microstructure of the Ti-10 wt.%Si samples show typical α-Ti + Ti_5Si_3 lath structures. The hardness of the Ti-10 wt.%Si was of about 650 kg/mm^2 at a pressure of 60 MPa at 1000 ºC.

Acknowledgments

This work was supported by a grant of the Human Resources Development Program (No. 20134030 200330) of the Korea Institute of Energy Technology Evaluation and Planning (KETEP), funded by the Korea government ministry of Trade, Industry and Energy.

References

1. R. Rosenkranz, G. Frommeyer, Mater. Sci. Eng. A152 (1992) 288-294.

2. C. L. Yeh, C. C. Hsu, J. Alloys & compd. 395 (2005) 53-59.
3. K. J. Park, J. K. Hong, S. K. Hwang, Metall. Trans. A28 (1997) 223-228.
4. H. C. Park, M. S. Kim, S. K. Hwang, Scripta Mater. 39 (1998) 1585-1591.
5. D. P. Riley, Intermetallics 14 (2006) 770-775.
6. D. M. Shah, D. Berczik, D. L. Alton, R. Hecht, Mater. Sci. Eng. A155 (1992) 45-47.
7. D. P. Riley, C. P. Oliver, E. H. Kihi, Intermetallics 14 (2006) 22-28.
8. T. Sandwick, K. Rajan, J. Electron. Mater. 19 (1990) 1193-1199.
9. R. Mitra, Metall. Trans. A29 (1998) 1629-1641.
10. K. Bhattacharya, J.J. Petrovic, J. Am. Ceram. Soc. 74 (1991) 2700-2708.
11. Y. Luo, S. Li, W. Pan, L. Li, Mater. Lett. 58 (2003) 150-154.
12. MP Harmer, RJ. Brook, J. Br. Ceram. Soc. 80 (1981) 147-149.
13. A. Morell, A. Mermosin, Bull. Am. Ceram. Soc. 59 (1980) 626-629.
14. Z. A. Munir, I. J. Shon, K. Yamazaki, K. Shoda, U.S. patent No 5, 794, 113 (1998).
15. I. J. Shon, Z. A. Munir, K. Yamazaki, K. Shoda, J. Am. Ceram. Soc. 79 (1996) 1875-1881.
16. I. J. Shon, H. C. Kim, D. H. Rho, Z. A. Munir, Mater. Sci & Eng. A 269 (1999) 129-135.
17. I. J. Shon, D. H. Rho, H. C. Kim, Z. A. Munir, J. Alloys & comp. 322 (2001) 120-125.
18. I. J. Shon, D. H. Rho, H. C. Kim, Met. & Mater. 6 (2000) 533-538.
19. C. D. Park, H. C. Kim, I. J. Shon, Z. A. Munir, J. Am. Ceram. Soc. 85 (2002) 2670-2676.
20. Zhang FL, Wang CY, Zhu M., Scripta Mater. 49(2003) 1123-1128.
21. Bernard-Granger M., Huizard C., J. Acta Mater, 55(10) (2007) 3493-3504.